Heterogeneous expression of the SARS-Coronavirus-2 receptor ACE2 in the human respiratory tract

Miguel Ortiz Bezara[1], Andrew Thurman[2], Alejandro Pezzulo[2], Mariah R. Leidinger[3], Julia A. Klesney-Tait[2], Philip H. Karp[2], Ping Tan[2], Christine Wohlford-Lenane[1], Paul B. McCray, Jr.[1*], David K. Meyerholz[3*]

Departments of Pediatrics[1], Internal Medicine[2], and Pathology[3]; University of Iowa College of Medicine, University of Iowa, Iowa City, IA USA

*Contributed equally

Correspondence:

David K. Meyerholz (david-meyerholz@uiowa.edu)

Paul B. McCray, Jr. (paul-mccray@uiowa.edu)

Running title: Expression of ACE2 in the human respiratory tract

Impact: The mapping of ACE2, the receptor for SARS-CoV-2, to specific anatomical regions and to particular cell types in the human respiratory tract will help guide future studies and provide molecular targets for antiviral therapies. We saw no increase of receptor expression in the presence of known risk factors for severe coronavirus disease 2019.

Author contributions:

Conceptualization and writing – original draft, M.O.B., P.B.M. and D.K.M.; Data curation, A.T.; Formal analysis, M.O.B., A.T., A.P. and D.K.M.; Investigation, A.T., A.P., M.R.L., C.W.-L. and D.K.M.; Visualization, M.O.B., A.T., D.K.M.; Resources, A.P., J.A.K.-T., P.H.K., P.T., P.B.M. and D.K.M.; Writing – review and editing, M.O.B, A.T., A.P., M.R.L., J.A.K.-T., P.H.K., P.T., C.W.-L., P.B.M. and D.K.M

This work is supported by the National Institutes of Health (NIH) Grant P01 AI060699; and the Pathology Core, which are partially supported by the Center for Gene Therapy for Cystic Fibrosis (NIH Grant P30 DK-54759), and the Cystic Fibrosis Foundation. P.B.M. is supported by the Roy J. Carver Charitable Trust.

Abstract:

Rationale: Zoonotically transmitted coronaviruses are responsible for three disease outbreaks since 2002, including the current coronavirus disease 2019 pandemic, caused by SARS-CoV-2. Its efficient transmission and range of disease severity raise questions regarding the contributions of virus-receptor interactions. ACE2 is a host ectopeptidase and the cellular receptor for SARS-CoV-2. Receptor expression on the cell surface facilitates viral binding and entry. However, reports of the abundance and distribution of ACE2 expression in the respiratory tract are limited and conflicting. *Objectives:* To determine ACE2 expression in the human respiratory tract and its association with demographic and clinical characteristics. *Methods:* Here, we systematically examined human upper and lower respiratory tract cells using single-cell RNA sequencing and immunohistochemistry to determine where the receptor is expressed. *Measurements and main results:* Our results reveal that ACE2 expression is highest within the sinonasal cavity and pulmonary alveoli, sites of presumptive viral transmission and severe disease development, respectively. In the lung parenchyma where severe disease occurs, ACE2 was found on the apical surface of a small subset of alveolar type II cells. We saw no increase of receptor expression in the presence of known risk factors for severe coronavirus disease 2019. *Conclusions:* The mapping of ACE2 to specific anatomical regions and to particular cell types in the respiratory tract will help guide future studies and provide molecular targets for antiviral therapies.

Word count: 223

Key words: Lung, expression, alveolar type II cells, ciliated cells

Main text:

Angiotensin-converting enzyme 2 (ACE2) is the cellular receptor for both severe acute respiratory syndrome coronavirus (SARS-CoV) and SARS-CoV-2 (1, 2). SARS-CoV caused a pneumonia outbreak in 2002-2003 with a mortality rate of 9.6% and over 800 deaths worldwide (3). SARS-CoV-2 is the etiologic agent of coronavirus disease 2019 (COVID-19) which was first recognized in December 2019 and has now reached pandemic proportions (2, 4). SARS-CoV-2 infection can be fatal, with the risk for increased disease severity correlating with advanced age and underlying comorbidities, while children and younger individuals have milder disease (5, 6). These trends could reflect age-related differences in ACE2 distribution and expression in the respiratory tract. Previous studies have variably shown ACE2 protein in the upper and lower respiratory tract, but cellular localization and distribution in human lung tissues have been inconsistent and contradictory (7-10) (Supplemental Table 1). *In vitro* studies demonstrate that ACE2 is expressed at the apical membrane of polarized airway epithelia, where it permits viral interaction and cell entry (10, 11). Here, we investigated the hypothesis that ACE2 expression drives disease severity in susceptible patient populations through enhanced abundance or distribution of ACE2 in different locations or cell types of the respiratory tract.

Severe COVID-19 is characterized by pneumonia and acute lung injury, so we first assessed publicly available scRNA-seq data from distal lung biopsies (12) and evaluated ACE2 transcript abundance in specific cell types. In the alveoli, most ACE2 transcripts were in alveolar type II (AT2) cells (89.5% of $ACE2^+$ cells) (Figure 1a), but specifically within a subset of these cells (1.2% of AT2 cells) (Figure 1b, Supplemental Figure 1a-b). Next, we optimized and validated ACE2 immunohistochemistry in extrapulmonary control tissues with high ACE2

expression (Supplemental Figure 2). We evaluated human lung tissues by immunohistochemistry (Supplemental Table 2 and Supplemental Table 3). Alveoli exhibited apical ACE2 protein in a small number (usually ~1% or less) of AT2 cells (Figure 1c), consistent with the results from scRNA-seq. The identity of these cells was confirmed by co-staining for surfactant protein-C. This $ACE2^+$ subset of AT2 cells was often observed within areas of alveolar collapse (Figures 1d-f), and these $ACE2^+$ cells were more plump and larger than $ACE2^-$ AT2 cells in the same tissue section (Figure 1g). AT2 cells can hypertrophy and proliferate following alveolar injury as they repopulate damaged alveolar type I (AT1) cells along the alveolar wall (13). Interestingly, alveolar macrophages were negative for ACE2 protein staining by immunohistochemistry, despite previous reports of ACE2 protein in these cells (Supplemental Table 1). The lack of ACE2 expression in macrophages was also confirmed by scRNA-seq data that revealed ACE2 mRNA transcripts in only 0.1% of macrophages, monocytes, or dendritic cells (Supplemental Figure 1a-b). The concordance between scRNA-seq and immunohistochemistry results provides evidence that ACE2 in the alveoli is primarily expressed in a subset of AT2 cells and that alveolar macrophages do not express ACE2.

Recent evidence indicates that proteases such as TMPRSS2 facilitate entry of SARS-CoV-2 into $ACE2^+$ cells (14). We evaluated scRNA-seq data and observed that TMPRSS2 was expressed in 35.5% of all AT2 cells (Figure 2a), and in 50.0% of $ACE2^+$ AT2 cells (Figure 2b). Additionally, we observed colocalization of ACE2 and TMPRSS2 on the apical membrane of AT2 cells (Figure 2c). These findings suggest that AT2 cells with apical ACE2 and TMPRSS2 could readily facilitate SARS-CoV-2 cellular infection and disease as seen in COVID-19 patients.

We next evaluated ACE2 in the conducting airways (trachea, bronchi, bronchioles). In the trachea and bronchi, apical ACE2 was rare and limited to ciliated cells (Figure 1h), similar to previous results in primary human airway epithelial cultures (11). In the submucosal glands of large airways, occasional serous cells and vessels near the acini were positive for ACE2 (Supplemental Figures 3a-b). In bronchioles, ACE2 was regionally localized (Figures 1i-k). These findings show nominal detection of ACE2, corresponding with the lack of primary airway disease (e.g. bronchitis, etc.) seen in COVID-19 patients.

Detection of ACE2 protein has had contrasting variability reported between several small studies (8, 10). In this larger study, we saw regional distribution of ACE2 protein varied between donors. We detected ACE2 protein in surface epithelium of large airways in only 12% of tracheal and 27% of bronchial tissues (Figure 3a). In the distal areas of the lung, ACE2 was more common, with positive protein detection in 36% of bronchiolar and 59% of alveolar samples (Figure 3a). A similar pattern of variable alveolar ACE2 was seen for mRNA transcripts in the scRNA-seq data, where 50% of donors showed low expression in AT2 cells, and the other 50% of donors showed high expression in the same cell type (Figure 3b). These findings suggest that ACE2 expression can vary between different lung regions and between individuals. Despite the heterogeneity of ACE2 detection between donors, 79% of subjects had positive ACE2 protein staining in at least one tissue. Given the large variability observed, it is possible that sampling limitations were responsible for the lack of ACE2 detection in the remaining 21% of donors. Additionally, we acknowledge that ACE2 could be expressed at levels below the limits of detection for scRNA-seq or immunohistochemistry.

Factors that could regulate ACE2 levels in the human lower respiratory tract include sex, age, or presence of comorbidities. The ACE2 gene resides on the X chromosome and therefore could be differentially regulated between males and females due to variable X-inactivation (15). Male sex correlates with increased levels of circulating ACE2 (reviewed in (16)) and early reports suggest males have increased COVID-19 severity (17). Advanced age and chronic comorbidities such as diabetes, cardiovascular disease, and renal disease are also associated with increased circulating ACE2 (reviewed in (16)), and these characteristics have also been associated with increased severity of COVID-19 (6, 18).

To evaluate whether the spatial distribution and abundance of ACE2 protein in the lower respiratory tract differed by age, sex, or presence of comorbidities, we scored tissues for ACE2 protein levels (Supplemental Table 2). In the cohort, neither age nor sex were associated with ACE2 protein detection (using the median age as cut-off) (Figures 3c-d). Since recent studies of COVID-19 infections suggested that young children may have reduced disease severity when infected by SARS-CoV-2 (6, 19), we compared lung tissue samples from children <10 years of age to those from older subjects (19-71 years of age) and found that ACE2 protein detection was higher in this subset of young children (Figure 3e). To test whether ACE2 distribution was affected by the presence of underlying diseases, we assessed the ACE2 localization pattern using tissues from subjects with chronic comorbidities (asthma, cardiovascular disease, chronic obstructive pulmonary disease, cystic fibrosis, diabetes, and smokers) and compared them to controls (Supplemental Table 2). The control group was similar in age to the chronic disease group (Figure 3f). We observed no significant differences between the two groups in ACE2

distribution, except for bronchioles, where ACE2 protein was reduced in the chronic disease group (Figure 3g, Supplemental Figure 3c). These results show that ACE2 levels in the respiratory tract did not increase in association with risk factors for severe COVID-19, such as advanced age and underlying chronic comorbidities. Instead, we saw increased ACE2 detection in children <10 years of age and in the small airways (bronchioles) of individuals without chronic comorbidities in our cohort. We note that not finding changes in receptor expression for SARS-CoV-2 is different from another severe coronavirus disease, MERS, where comorbidities were observed to increase its receptor detection in respiratory tissues (20, 21).

Given the unexpected heterogeneity in the lower respiratory tract, we also investigated ACE2 in the upper respiratory tract. We studied ACE2 gene expression using publicly available scRNA-seq data from nasal brushing and nasal turbinate samples (22) and observed ACE2 mRNA transcripts in 2-6% of epithelial cells (Supplemental Figure 4a-d). We then studied nasal biopsy tissues and found that ACE2 protein was detected in all tissue samples and, when present, was seen exclusively on the apical surface of ciliated cells. Distribution varied regionally based on the characteristics of the epithelium, with rare detection in thicker ciliated pseudostratified epithelium, and more abundant expression in thinner epithelium (Figures 4a-g). Thinner epithelial height is recognized in specific regions including the floor of the nasal cavity, meatuses, and paranasal sinuses (23). Both, epithelial heterogeneity and undefined biopsy sites in sinonasal cavity, limited direct comparisons between scRNA-seq results and protein staining. Additionally, it is possible ACE2 protein cannot be detected in all cell types with ACE2 mRNA due to low expression, rapid protein turnover, or post-transcriptional regulation. The sinonasal cavity is an interface between the respiratory tract and the environment. High SARS-CoV-2

173 viral loads can be detected in nasal swabs from infected patients (24), consistent with our ACE2
174 expression data. This reservoir of ACE2$^+$ cells may facilitate the reported transmission from
175 individuals who have very mild or asymptomatic disease (25).
176
177 Through study of these respiratory tissues, we found that ACE2 protein was most
178 consistently detected in the sinonasal cavity and the alveoli. Expression of ACE2 in the nasal
179 cavity could explain the high transmissibility of SARS-CoV-2 and HCoV-NL63, a cold-related
180 coronavirus, which also uses ACE2 as a receptor. One mystery is why SARS-CoV, which also
181 uses ACE2, was apparently unable to easily transmit from human-to-human (26). Whether this
182 represents differences in the interactions of SARS-CoV and SARS-CoV-2 with co-receptors (27)
183 or other factors in the nasal cavity remains to be investigated. SARS-CoV and SARS-CoV-2
184 both replicate in the lungs (28, 29), consistent with the ACE2 distribution defined in this and
185 suggested by previous studies (9, 10). Most of the ACE2 expression in the lung was found in
186 AT2 cells, which are targets for SARS-CoV (30) and presumably SARS-CoV-2 (29). Given that
187 AT2 cells are critical for surfactant protein production and serve as progenitor cells for the AT1
188 cells, damage to these cells could contribute to acute lung injury (31), which is a common feature
189 of severe COVID-19 (5). Infection of AT2 cells could disrupt epithelial integrity leading to
190 alveolar edema, and facilitate viral spread to other epithelial cells or to ACE2$^+$ interstitial
191 cells/vessels for systemic virus dissemination, given that SARS-CoV-2 has been detected in
192 blood (32). Furthermore, cell-to-cell spread of coronaviruses after initial infection could also
193 occur via receptor-independent mechanisms related to the fusogenic properties of the S protein
194 (33). It is interesting that computerized tomography studies of early disease in people with

COVID-19 demonstrate patchy ground glass opacities in the peripheral and posterior lungs, regions that are more susceptible to collapse (34).

The elevated detection of ACE2 protein in demographic pools with expected low risk for severe COVID-19 was unexpected and suggests alternative explanations. First, the potential relationship between ACE2 in the respiratory tract and severe COVID-19 is likely complex. On one hand, more receptor availability could enhance viral entry into cells and worsen disease outcomes; alternatively, ACE2 may play a protective role in acute lung injury (35-37) and therefore could improve disease outcomes. Our data would support the latter and implicate a dualistic role for ACE2 as both a viral receptor and a protective agent in acute lung injury. Additionally, ACE2 exists in cell-associated and soluble forms (38). It is possible that greater ACE2 expression could result in increased soluble ACE2 in respiratory secretions where it might act as a decoy receptor and reduce virus entry (1, 39). Second, other factors such as TMPRSS2 expression might be more important in regulating disease severity. TMPRSS2 on the apical membrane of AT2 cells might facilitate SARS-CoV-2 entry when ACE2 is rare or even below the limit of detection in this study.

In summary, we find that ACE2 protein has heterogeneous expression in the respiratory tract with higher ACE2 detection in the sinonasal epithelium and AT2 cells that correlates with putative sites for transmission and severe disease, respectively. The small subset of $ACE2^{+}$ AT2 cells in the lung could be further studied to reveal factors regulating ACE2 expression and clarify potential targets for antiviral therapies.

Word count: 2139

Acknowledgements:

We thank our laboratory members and colleagues Stanley Perlman, Robert Robinson, and Thomas Gallagher for their helpful discussion and technical assistance.

Competing interest declaration:

The authors declare no competing interests.

Materials and methods:

Tissues:

Studies on human tissues were approved by the institutional review board of the University of Iowa. Tissues included nasal biopsies (n=3, deidentified and lacked evidence of significant disease or cancer), lung donors, primary cell cultures (40), and autopsy tissues (control tissues) that were selected from archival repositories as formalin-fixed paraffin-embedded blocks. Lung cases were selected to comprise two case study groups: 1) Chronic disease group was defined as having chronic comorbidities including: asthma, cardiovascular disease, chronic obstructive pulmonary disease, cystic fibrosis, diabetes, and smoking. 2) Control group was defined as lacking these chronic comorbidities and lacking clinical lung disease. The cumulative cohort included 29 cases (15 chronic comorbidities and 14 controls) with a broad range of ages (0.5 – 71 years) and both sexes were represented (13 female and 16 male). For these lungs, if a trachea or bronchus tissue block was available from the same case – these were included as well (Supplemental Table 2). Bronchioles were observed in most lung sections and were defined as intrapulmonary airways lacking evidence of cartilage or submucosal glands (41).

Immunohistochemistry and immunofluorescence:

All formalin-fixed paraffin-embedded tissues were sectioned (~4 μm) and hydrated through a series of xylene and alcohol baths to water. Immunohistochemistry was then applied to these studies to evaluate angiotensin-converting enzyme 2 (ACE2) (11), allograft inflammatory factor 1 (AIF1, also known as IBA1) (42), surfactant protein C (SP-C) (43) and mucin 5B (MUC5B) (42). For more specifics about the reagents please see Supplemental Table 3.

For immunofluorescence, formalin-fixed and paraffin-embedded human lung blocks were sectioned (~4 μm). Slides were baked (55°C x 15 min) and then deparaffinized (hydrated) in a series of xylene and progressive alcohol baths. Antigen retrieval was performed using Antigen Unmasking Solution (1:100, #H-3300) in citrate buffer (pH 6.0) solution to induce epitope retrieval (5 min x 3 times) in the microwave. Slides were washed (PBS, 3 times, 5 min each) and a PAP pen used to encircle the tissue. Slides were blocked with background blocking solution (2% BSA in Superblock 1 hr in humid chamber). Primary antibodies anti-ACE2 (1:100, Mouse monoclonal, MAB933, R&D Systems, Minneapolis, MN USA) and anti-TMPRSS2 (1:200, Rabbit monoclonal, #ab92323, Abcam, Cambridge, MA USA) were diluted in blocking solution (2% BSA in Superblock overnight 4°C). Secondary antibodies anti-mouse Alexa568 (for ACE2) and anti-rabbit Alexa488 (for TMPRSS2) were applied at a concentration of 1:600 for 1 hour at room temperature. Slides were washed and mounted with Vectashield containing DAPI.

Tissue scoring:

Stained tissue sections were examined for ACE2 localization using a post-examination method for masking and scored by a masked pathologist following principles for reproducible tissue scores (44). The initial examination showed a low incidence of ACE2 staining for various tissues, so the following ordinal scoring system was employed to quantify number of staining-positive cells: 0 = below the limit of detection; 1 = <1%; 2 = 1-33%; 3 = 34-66%; and 4 = >66% of cells. For these anatomic regions (e.g. airway or alveoli), cell counts for each tissue were made to know the population density per microscopic field to make reproducible interpretations. For determination of AT2 cell size, ACE2 and SP-C protein immunostaining were evaluated on

the same lung tissue section for each case. A region of minimally diseased lung was examined and SP-C$^+$ AT2 cells were measured for diameter in the plane perpendicular to the basement membrane. Similar measurements were then made for ACE2$^+$/SP-C$^+$ cells.

Analysis of single cell RNA sequencing data:

Single cell RNA sequencing data sets were accessed from Gene Expression Omnibus (GEO) series GSE121600 (22) and GSE122960 (12). For GSE121600, raw H5 files for bronchial biopsy (GSM3439925), nasal brushing (GSM3439926), and turbinate (GSM3439927) samples were downloaded, and barcodes with less than 1000 unique molecular identifiers (UMIs) were discarded. For GSE122960, filtered H5 files for eight lung transplant donor samples from lung parenchyma (GSM3489182, GSM3489185, GSM3489187, GSM3489189, GSM3489191, GSM3489193, GSM3489195, GSM3489197) were downloaded, and all barcodes were retained. The eight donors varied from 21-63 years of age (median age = 48) and were composed of five African American, one Asian, and two white donors, and 2 active, 1 former, and 5 never smokers. Gene count matrices from the eight donors were aggregated for analysis.

All four data sets (bronchial biopsy, nasal brushing, turbinate, and lung parenchyma) were processed in a similar manner. Gene-by-barcode count matrices were normalized, log-transformed, and scaled followed by dimension reduction using principal components analysis (PCA). Principal components were used to obtain uniform manifold approximation and projection (UMAP) visualizations, and cells were clustered using a shared nearest neighbor (SNN) approach. Cell types associated with each cluster were identified by determining marker genes for each cluster. All analyses were performed using R package Seurat version 3.1.1 (45).

In the nasal brushing sample, we were unable to associate a cell type with one cluster containing 776 cells (16.5%) due to low UMIs, so these cells were discarded. For the bronchial biopsy sample, 82.4% of cells had less than 3,000 UMIs, so we lacked confidence in assigned cell types, and thus results were not reported.

For the lung parenchyma data, gene expression in alveolar type II cells for a single donor was quantified by summing up gene counts for all alveolar type II cells and dividing by total UMIs for all alveolar type II cells to get normalized counts, followed by rescaling the normalized counts to obtain counts per million (CPM).

Statistical analyses:

Statistical analyses for group comparisons and tissue scoring data were performed using GraphPad Prism version 8 (GraphPad Software, La Jolla, CA USA). For group comparisons, Mann Whitney U tests or T-tests were used for group comparisons as appropriate and Cochran-Armitage test for trend was used to compare ACE2 protein detection in different tissues.

References:

1. Li W, Moore MJ, Vasilieva N, Sui J, Wong SK, Berne MA, Somasundaran M, Sullivan JL, Luzuriaga K, Greenough TC, Choe H, Farzan M. Angiotensin-converting enzyme 2 is a functional receptor for the SARS coronavirus. *Nature* 2003; 426: 450-454.
2. Zhou P, Yang XL, Wang XG, Hu B, Zhang L, Zhang W, Si HR, Zhu Y, Li B, Huang CL, Chen HD, Chen J, Luo Y, Guo H, Jiang RD, Liu MQ, Chen Y, Shen XR, Wang X, Zheng XS, Zhao K, Chen QJ, Deng F, Liu LL, Yan B, Zhan FX, Wang YY, Xiao GF, Shi ZL. A pneumonia outbreak associated with a new coronavirus of probable bat origin. *Nature* 2020.
3. Lam CW, Chan MH, Wong CK. Severe acute respiratory syndrome: clinical and laboratory manifestations. *Clin Biochem Rev* 2004; 25: 121-132.
4. Wilder-Smith A, Chiew CJ, Lee VJ. Can we contain the COVID-19 outbreak with the same measures as for SARS? *Lancet Infect Dis* 2020.
5. Zhou F, Yu T, Du R, Fan G, Liu Y, Liu Z, Xiang J, Wang Y, Song B, Gu X, Guan L, Wei Y, Li H, Wu X, Xu J, Tu S, Zhang Y, Chen H, Cao B. Clinical course and risk factors for mortality of adult inpatients with COVID-19 in Wuhan, China: a retrospective cohort study. *Lancet* 2020.
6. Guan WJ, Ni ZY, Hu Y, Liang WH, Ou CQ, He JX, Liu L, Shan H, Lei CL, Hui DSC, Du B, Li LJ, Zeng G, Yuen KY, Chen RC, Tang CL, Wang T, Chen PY, Xiang J, Li SY, Wang JL, Liang ZJ, Peng YX, Wei L, Liu Y, Hu YH, Peng P, Wang JM, Liu JY, Chen Z, Li G, Zheng ZJ, Qiu SQ, Luo J, Ye CJ, Zhu SY, Zhong NS, China Medical Treatment Expert Group for C. Clinical Characteristics of Coronavirus Disease 2019 in China. *N Engl J Med* 2020.
7. Bertram S, Glowacka I, Muller MA, Lavender H, Gnirss K, Nehlmeier I, Niemeyer D, He Y, Simmons G, Drosten C, Soilleux EJ, Jahn O, Steffen I, Pohlmann S. Cleavage and activation of the severe acute respiratory syndrome coronavirus spike protein by human airway trypsin-like protease. *J Virol* 2011; 85: 13363-13372.
8. Bertram S, Heurich A, Lavender H, Gierer S, Danisch S, Perin P, Lucas JM, Nelson PS, Pohlmann S, Soilleux EJ. Influenza and SARS-coronavirus activating proteases TMPRSS2 and HAT are expressed at multiple sites in human respiratory and gastrointestinal tracts. *PLoS One* 2012; 7: e35876.
9. Hamming I, Timens W, Bulthuis ML, Lely AT, Navis G, van Goor H. Tissue distribution of ACE2 protein, the functional receptor for SARS coronavirus. A first step in understanding SARS pathogenesis. *J Pathol* 2004; 203: 631-637.
10. Ren X, Glende J, Al-Falah M, de Vries V, Schwegmann-Wessels C, Qu X, Tan L, Tschernig T, Deng H, Naim HY, Herrler G. Analysis of ACE2 in polarized epithelial cells: surface expression and function as receptor for severe acute respiratory syndrome-associated coronavirus. *J Gen Virol* 2006; 87: 1691-1695.
11. Jia HP, Look DC, Shi L, Hickey M, Pewe L, Netland J, Farzan M, Wohlford-Lenane C, Perlman S, McCray PB, Jr. ACE2 receptor expression and severe acute respiratory syndrome coronavirus infection depend on differentiation of human airway epithelia. *J Virol* 2005; 79: 14614-14621.
12. Reyfman PA, Walter JM, Joshi N, Anekalla KR, McQuattie-Pimentel AC, Chiu S, Fernandez R, Akbarpour M, Chen CI, Ren Z, Verma R, Abdala-Valencia H, Nam K, Chi M, Han S, Gonzalez-Gonzalez FJ, Soberanes S, Watanabe S, Williams KJN, Flozak AS, Nicholson

TT, Morgan VK, Winter DR, Hinchcliff M, Hrusch CL, Guzy RD, Bonham CA, Sperling AI, Bag R, Hamanaka RB, Mutlu GM, Yeldandi AV, Marshall SA, Shilatifard A, Amaral LAN, Perlman H, Sznajder JI, Argento AC, Gillespie CT, Dematte J, Jain M, Singer BD, Ridge KM, Lam AP, Bharat A, Bhorade SM, Gottardi CJ, Budinger GRS, Misharin AV. Single-Cell Transcriptomic Analysis of Human Lung Provides Insights into the Pathobiology of Pulmonary Fibrosis. *Am J Respir Crit Care Med* 2019; 199: 1517-1536.

13. Olajuyin AM, Zhang X, Ji HL. Alveolar type 2 progenitor cells for lung injury repair. *Cell Death Discov* 2019; 5: 63.
14. Hoffmann M, Kleine-Weber H, Schroeder S, Kruger N, Herrler T, Erichsen S, Schiergens TS, Herrler G, Wu NH, Nitsche A, Muller MA, Drosten C, Pohlmann S. SARS-CoV-2 Cell Entry Depends on ACE2 and TMPRSS2 and Is Blocked by a Clinically Proven Protease Inhibitor. *Cell* 2020.
15. Carrel L, Willard HF. X-inactivation profile reveals extensive variability in X-linked gene expression in females. *Nature* 2005; 434: 400-404.
16. Anguiano L, Riera M, Pascual J, Soler MJ. Circulating ACE2 in Cardiovascular and Kidney Diseases. *Curr Med Chem* 2017; 24: 3231-3241.
17. Mo P, Xing Y, Xiao Y, Deng L, Zhao Q, Wang H, Xiong Y, Cheng Z, Gao S, Liang K, Luo M, Chen T, Song S, Ma Z, Chen X, Zheng R, Cao Q, Wang F, Zhang Y. Clinical characteristics of refractory COVID-19 pneumonia in Wuhan, China. *Clin Infect Dis* 2020.
18. Lu Q, Shi Y. Coronavirus disease (COVID-19) and neonate: What neonatologist need to know. *J Med Virol* 2020.
19. Dong Y, Mo X, Hu Y, Qi X, Jiang F, Jiang Z, Tong S. Epidemiological Characteristics of 2143 Pediatric Patients With 2019 Coronavirus Disease in China. *Pediatrics* 2020.
20. Meyerholz DK, Lambertz AM, McCray PB, Jr. Dipeptidyl Peptidase 4 Distribution in the Human Respiratory Tract: Implications for the Middle East Respiratory Syndrome. *Am J Pathol* 2016; 186: 78-86.
21. Seys LJM, Widagdo W, Verhamme FM, Kleinjan A, Janssens W, Joos GF, Bracke KR, Haagmans BL, Brusselle GG. DPP4, the Middle East Respiratory Syndrome Coronavirus Receptor, is Upregulated in Lungs of Smokers and Chronic Obstructive Pulmonary Disease Patients. *Clin Infect Dis* 2018; 66: 45-53.
22. Ruiz Garcia S, Deprez M, Lebrigand K, Cavard A, Paquet A, Arguel MJ, Magnone V, Truchi M, Caballero I, Leroy S, Marquette CH, Marcet B, Barbry P, Zaragosi LE. Novel dynamics of human mucociliary differentiation revealed by single-cell RNA sequencing of nasal epithelial cultures. *Development* 2019; 146.
23. Sternberg SS. Histology for Pathologists. Philadelphia, PA USA: Lippincott-Raven Publishers; 1997.
24. Wang W, Xu Y, Gao R, Lu R, Han K, Wu G, Tan W. Detection of SARS-CoV-2 in Different Types of Clinical Specimens. *JAMA* 2020.
25. Bai Y, Yao L, Wei T, Tian F, Jin DY, Chen L, Wang M. Presumed Asymptomatic Carrier Transmission of COVID-19. *JAMA* 2020.
26. Wang Y, Wang Y, Chen Y, Qin Q. Unique epidemiological and clinical features of the emerging 2019 novel coronavirus pneumonia (COVID-19) implicate special control measures. *J Med Virol* 2020.

27. Wrapp D, Wang N, Corbett KS, Goldsmith JA, Hsieh CL, Abiona O, Graham BS, McLellan JS. Cryo-EM structure of the 2019-nCoV spike in the prefusion conformation. *Science* 2020; 367: 1260-1263.
28. Yen YT, Liao F, Hsiao CH, Kao CL, Chen YC, Wu-Hsieh BA. Modeling the early events of severe acute respiratory syndrome coronavirus infection in vitro. *J Virol* 2006; 80: 2684-2693.
29. Zhang H, Zhou P, Wei Y, Yue H, Wang Y, Hu M, Zhang S, Cao T, Yang C, Li M, Guo G, Chen X, Chen Y, Lei M, Liu H, Zhao J, Peng P, Wang CY, Du R. Histopathologic Changes and SARS-CoV-2 Immunostaining in the Lung of a Patient With COVID-19. *Ann Intern Med* 2020.
30. Mossel EC, Wang J, Jeffers S, Edeen KE, Wang S, Cosgrove GP, Funk CJ, Manzer R, Miura TA, Pearson LD, Holmes KV, Mason RJ. SARS-CoV replicates in primary human alveolar type II cell cultures but not in type I-like cells. *Virology* 2008; 372: 127-135.
31. Ware LB, Matthay MA. The acute respiratory distress syndrome. *N Engl J Med* 2000; 342: 1334-1349.
32. Chen W, Lan Y, Yuan X, Deng X, Li Y, Cai X, Li L, He R, Tan Y, Deng X, Gao M, Tang G, Zhao L, Wang J, Fan Q, Wen C, Tong Y, Tang Y, Hu F, Li F, Tang X. Detectable 2019-nCoV viral RNA in blood is a strong indicator for the further clinical severity. *Emerg Microbes Infect* 2020; 9: 469-473.
33. Gallagher TM, Buchmeier MJ, Perlman S. Dissemination of MHV4 (strain JHM) infection does not require specific coronavirus receptors. *Adv Exp Med Biol* 1993; 342: 279-284.
34. Song F, Shi N, Shan F, Zhang Z, Shen J, Lu H, Ling Y, Jiang Y, Shi Y. Emerging 2019 Novel Coronavirus (2019-nCoV) Pneumonia. *Radiology* 2020; 295: 210-217.
35. Gu H, Xie Z, Li T, Zhang S, Lai C, Zhu P, Wang K, Han L, Duan Y, Zhao Z, Yang X, Xing L, Zhang P, Wang Z, Li R, Yu JJ, Wang X, Yang P. Angiotensin-converting enzyme 2 inhibits lung injury induced by respiratory syncytial virus. *Sci Rep* 2016; 6: 19840.
36. Imai Y, Kuba K, Rao S, Huan Y, Guo F, Guan B, Yang P, Sarao R, Wada T, Leong-Poi H, Crackower MA, Fukamizu A, Hui CC, Hein L, Uhlig S, Slutsky AS, Jiang C, Penninger JM. Angiotensin-converting enzyme 2 protects from severe acute lung failure. *Nature* 2005; 436: 112-116.
37. Zou Z, Yan Y, Shu Y, Gao R, Sun Y, Li X, Ju X, Liang Z, Liu Q, Zhao Y, Guo F, Bai T, Han Z, Zhu J, Zhou H, Huang F, Li C, Lu H, Li N, Li D, Jin N, Penninger JM, Jiang C. Angiotensin-converting enzyme 2 protects from lethal avian influenza A H5N1 infections. *Nat Commun* 2014; 5: 3594.
38. Lambert DW, Yarski M, Warner FJ, Thornhill P, Parkin ET, Smith AI, Hooper NM, Turner AJ. Tumor necrosis factor-alpha convertase (ADAM17) mediates regulated ectodomain shedding of the severe-acute respiratory syndrome-coronavirus (SARS-CoV) receptor, angiotensin-converting enzyme-2 (ACE2). *J Biol Chem* 2005; 280: 30113-30119.
39. Hofmann H, Geier M, Marzi A, Krumbiegel M, Peipp M, Fey GH, Gramberg T, Pohlmann S. Susceptibility to SARS coronavirus S protein-driven infection correlates with expression of angiotensin converting enzyme 2 and infection can be blocked by soluble receptor. *Biochem Biophys Res Commun* 2004; 319: 1216-1221.
40. Itani OA, Chen JH, Karp PH, Ernst S, Keshavjee S, Parekh K, Klesney-Tait J, Zabner J, Welsh MJ. Human cystic fibrosis airway epithelia have reduced Cl- conductance but not increased Na+ conductance. *Proc Natl Acad Sci U S A* 2011; 108: 10260-10265.

41. Meyerholz DK, Suarez CJ, Dintzis SM, Frevert CW. Comparative Anatomy and Histology: A Mouse, Rat and Human Atlas. Academic Press - Elsevier; 2018.
42. Meyerholz DK, Lambertz AM, Reznikov LR, Ofori-Amanfo GK, Karp PH, McCray PB, Jr., Welsh MJ, Stoltz DA. Immunohistochemical Detection of Markers for Translational Studies of Lung Disease in Pigs and Humans. *Toxicol Pathol* 2016; 44: 434-441.
43. Krishnamurthy S, Wohlford-Lenane C, Kandimalla S, Sartre G, Meyerholz DK, Theberge V, Hallee S, Duperre AM, Del'Guidice T, Lepetit-Stoffaes JP, Barbeau X, Guay D, McCray PB, Jr. Engineered amphiphilic peptides enable delivery of proteins and CRISPR-associated nucleases to airway epithelia. *Nat Commun* 2019; 10: 4906.
44. Meyerholz DK, Beck AP. Principles and approaches for reproducible scoring of tissue stains in research. *Lab Invest* 2018; 98: 844-855.
45. Stuart T, Butler A, Hoffman P, Hafemeister C, Papalexi E, Mauck WM, 3rd, Hao Y, Stoeckius M, Smibert P, Satija R. Comprehensive Integration of Single-Cell Data. *Cell* 2019; 177: 1888-1902 e1821.

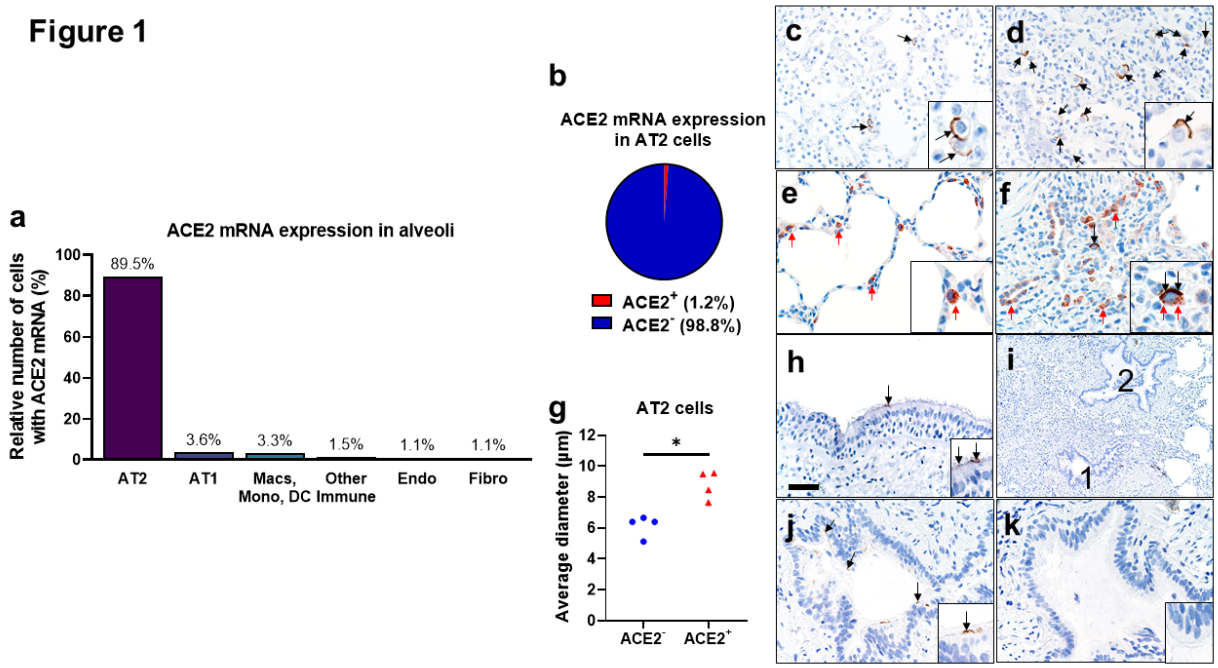

Figure 1. ACE2 expression in human lower respiratory tract. **a, b**) Single-cell RNA sequencing reanalysis of ACE2 expression in alveoli from lung parenchyma samples [14]. Airway cells (basal, mitotic, ciliated, club) are not shown. **a**) 89.5% of the cells expressing ACE2 mRNA in the alveoli are alveolar type II cells. **b**) Only 1.2% of alveolar type II cells express ACE2 mRNA. **c-f**, **h-k**) Detection of ACE2 protein (brown color, black arrows and insets) in representative sections of lower respiratory tract regions and tissue scoring (see Supplemental Table 2) (**g**). **c, d**) Alveolar regions had uncommon to regional polarized apical staining of solitary epithelial cells (**c**) that (when present) were more readily detected in collapsed regions of lung (**d**). **e, f**) SP-C (red arrows, inset) and ACE2 (black arrows, inset) dual immunohistochemistry on the same tissue sections. **e**) Non-collapsed regions had normal SP-C$^+$ AT2 cells lacking ACE2. **f**) Focal section of peri-airway remodeling and collapse with several SP-C$^+$ (red arrows) AT2 cells, but only a small subset of AT2 cells had prominent apical ACE2 protein (black arrows, inset). **g**) SP-C$^+$/ACE2$^+$ AT2 cells were often larger than SP-C$^+$/ACE2$^-$ AT2 cells from same lung sections (see also **d** and **e** insets) indicative of AT2 hypertrophy, each data point represents the average

475 value for each case from 5-10 cell measurements per group, P=0.0014, paired T-test. **h**) Large
476 airways (trachea and bronchi) exhibited rare ACE2 protein on the apical surface of ciliated cells.
477 **i-k**) Small airways (bronchioles) exhibited uncommon to localized apical ACE2 protein in
478 ciliated cells (**j**, #1 in **i**) while the adjacent bronchioles (**k**, #2 in **i**) lacked protein. AT2: alveolar
479 type II. AT1: alveolar type I. Macs: Macrophages. Mono: Monocytes. DC: dendritic cells. Other
480 immune cells: B cells, mast cells, natural killer/T cells. Endo: Endothelial. Fibro:
481 Fibroblasts/myofibroblasts. Bar = 35 (b-e, g), 140 (h) and 70 μm (i, j).
482

Figure 2

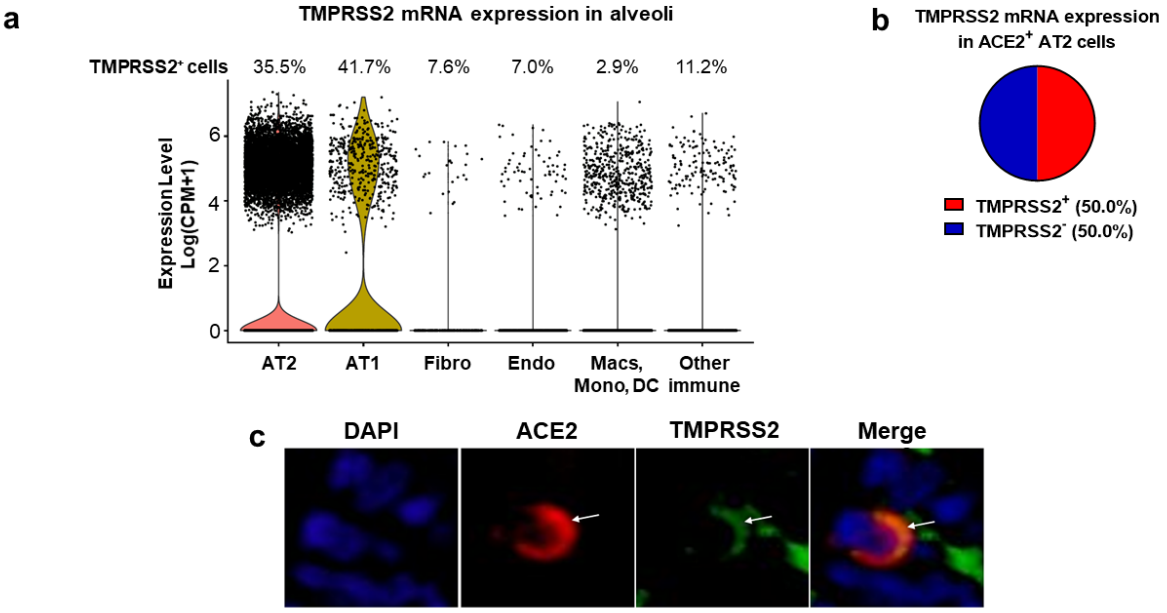

Figure 2. TMPRSS2 expression in the alveoli. **a, b**) Single-cell RNA sequencing reanalyses of TMPRSS2 expression in alveoli from lung parenchyma [14]. **a**) Percentage of TMPRSS2$^+$ cells within each cell type shows TMPRSS2 transcripts in 35.5% of alveolar type II cells. Airway cells (basal, mitotic, ciliated, club) are not shown. Violin plots represent expression, each data point denotes a cell. **b**) TMPRSS2 expression in ACE2$^+$ alveolar type II cells. **c**) Immunofluorescence of alveoli shows apical colocalization of ACE2 and TMPRSS2 (white arrows). AT2: alveolar type II. AT1: alveolar type I. Macs: Macrophages. Mono: Monocytes. DC: dendritic cells. Other immune cells: B cells, mast cells, natural killer/T cells. Endo: Endothelial. Fibro: Fibroblasts/myofibroblasts. CPM: counts per million.

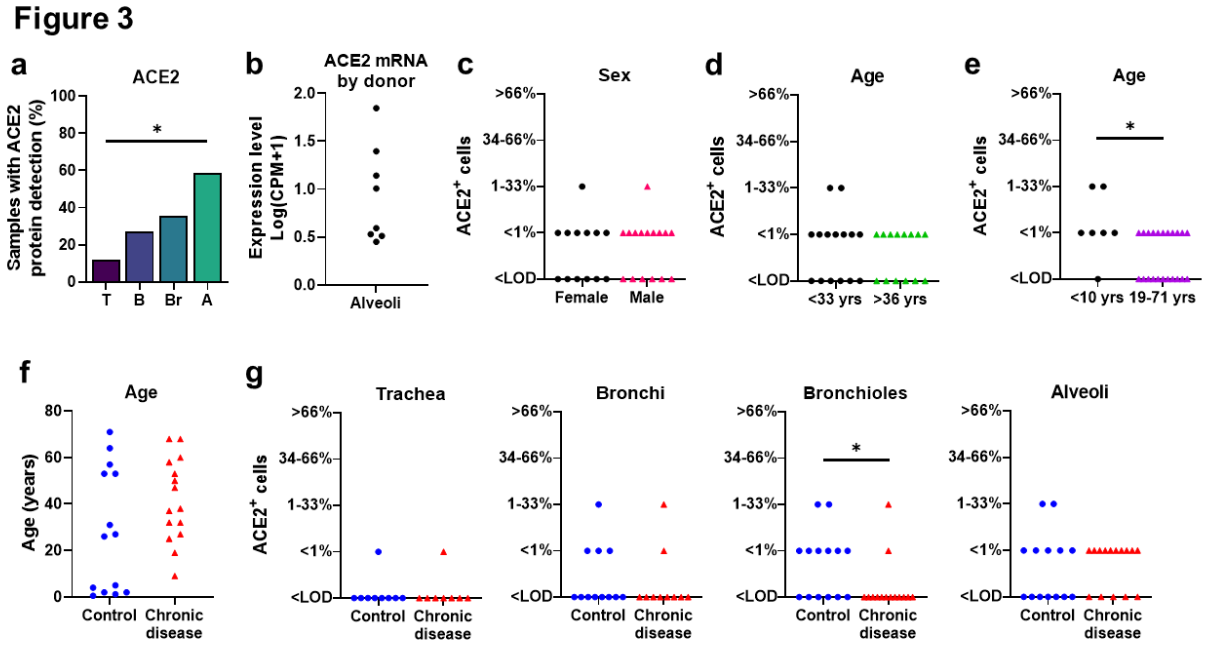

494

495 **Figure 3.** ACE2 localization and scores in respiratory tissues. **a**) ACE2 protein had progressively
496 increased detection between donors in tissues from trachea (T), bronchi (B), bronchioles (Br), to
497 alveoli (A), (P=0.0009, Cochran-Armitage test for trend). **b**) ACE2 mRNA expression in the
498 alveoli varied between donors. **c-d**) ACE2 protein scores from lung samples showed no
499 differences based on sex or lower vs. upper ages (using median age as a cut-off) (A, P=0.7338
500 and B, P=0.7053, Mann-Whitney U test). **e**) ACE2 protein scores were elevated in young
501 children (<10 yrs) compared to the remaining subjects (19-71 yrs) (P=0.0282 Mann-Whitney U
502 test). **f**) Control and chronic disease groups did not have any significant differences in age
503 (P=0.1362 Mann-Whitney U test). **g**) ACE2 protein scores for trachea, bronchi, bronchiole, and
504 alveoli in control versus chronic disease groups (P= >0.9999, 0.6263, 0.0433, and 0.7359,
505 respectively, Mann-Whitney U test). CPM: counts per million. LOD: Limit of detection.

506

Figure 4

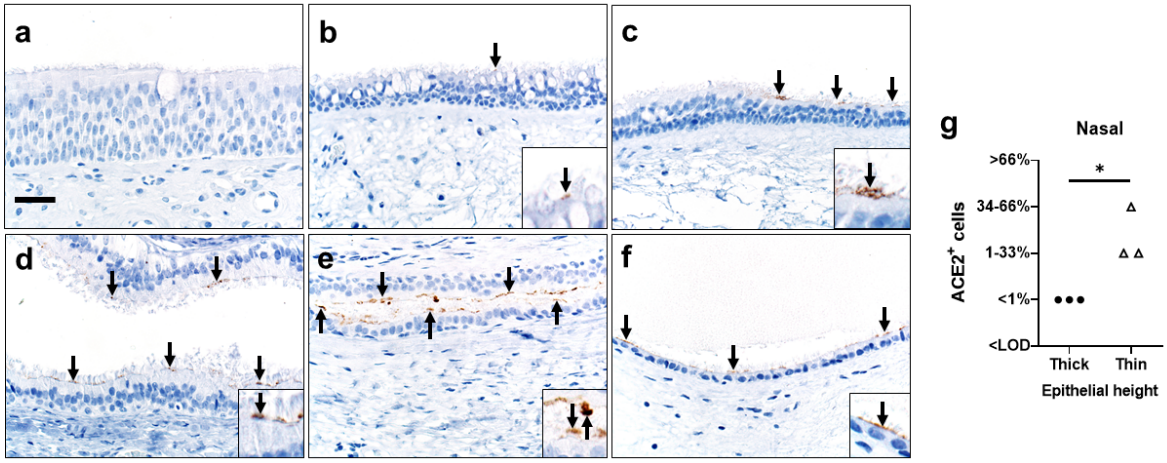

507

508 **Figure 4.** Detection of ACE2 protein (brown color, arrows and insets, **a-f**) and tissue scoring (**g**)
509 in representative sections of nasal tissues. **a, b**) In thick pseudostratified epithelium (PSE) ACE2
510 protein was absent (**a**) to rare (**b**) and apically located on ciliated cells. **c**) Tissue section shows a
511 transition zone from thick (left side, > ~4 nuclei) to thin (right side, ≤ ~4 nuclei) PSE and ACE2
512 protein was restricted to the apical surface of the thin PSE. **d-f**) ACE2 protein was detected
513 multifocally on the apical surface of ciliated cells in varying types of thin PSE, even to simple
514 cuboidal epithelium (**f**). Bar = 30 μm. **g**) ACE2 protein detection scores for each subject were
515 higher in thin than thick epithelium, (P=0.05, Mann-Whitney U test). LOD: Limit of detection.

516

517 **Supplemental information:**

Supplemental Figure 1

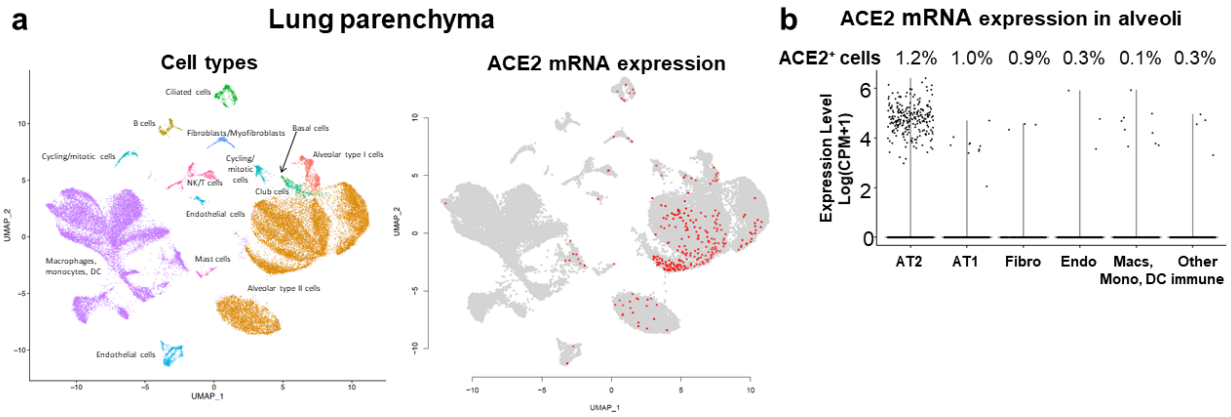

518

519 **Supplemental Figure 1.** Single-cell RNA sequencing reanalyses of ACE2 expression in lung
520 parenchyma [14]. **a**) Uniform manifold approximation and projection (UMAP) visualizations. Cells
521 were clustered using a shared nearest neighbor (SNN) approach. Cell types associated with each
522 cluster were identified by determining marker genes for each cluster. Each data point denotes a
523 cell. On the right panel, cells expressing ACE2 are shown in red. **b**) Violin plots representing
524 ACE2 expression in the alveoli. Airway cells (basal, mitotic, ciliated, club) are not shown.
525 Percentage of $ACE2^+$ cells within each cell type shows ACE2 transcripts in 1.2% of alveolar
526 type II cells and in 0.1% of macrophages, monocytes, or dendritic cells. Each data point denotes
527 a cell, most cells have no expression (0). AT2: alveolar type II. AT1: alveolar type I. Macs:
528 Macrophages. Mono: Monocytes. DC: dendritic cells. Other immune cells: B cells, mast cells,
529 natural killer/T cells. Endo: Endothelial. Fibro: Fibroblasts/myofibroblasts. NK: Natural killer.
530 CPM: Counts per million.

531

Supplemental Figure 2

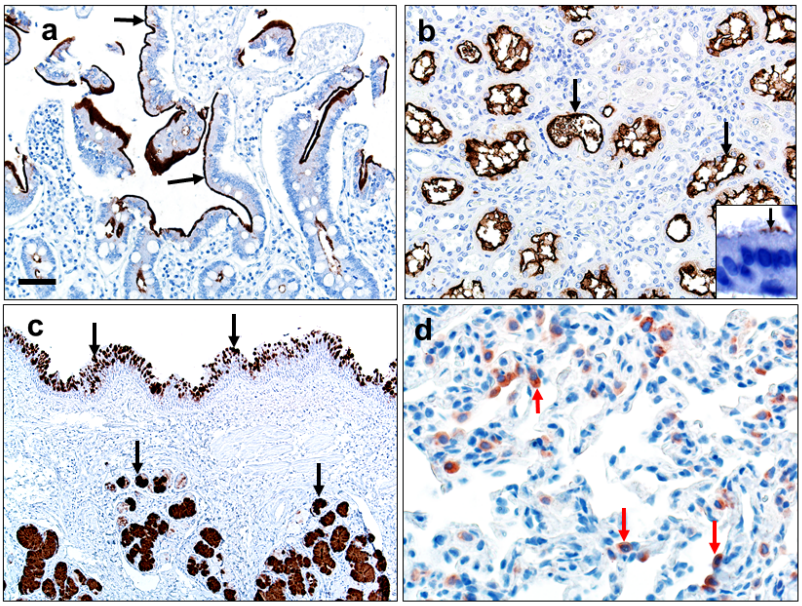

Supplemental Figure 2. Quality controls for ACE2 immunohistochemistry technique (**a, b**) and tissue quality (**c, d**). **a, b**) ACE2 protein (brown color, black arrows) was detected along the apical surface of small intestine enterocytes (**a**), renal tubule epithelium (**b**), and ciliated cells (**b, inset**) of primary airway cell cultures. These findings demonstrate specific detection of ACE2 protein in cells/tissues consistent with known ACE2 expression. **c**) Representative immunostaining of bronchus detected abundant MUC5B protein (brown color, black arrows) in mucous cells of surface epithelium (top) and submucosal glands (bottom). **d**) Representative sections of alveoli had SP-C^{+} alveolar type II cells (red color, red arrows). These results (**c, d**) demonstrate the tissues were intact and that immunostaining can be used to detect native airway (**c**) and lung (**d**) proteins. Bar = 40 (a, b), 80 (c), and 20 μm (d).

Supplemental Figure 3

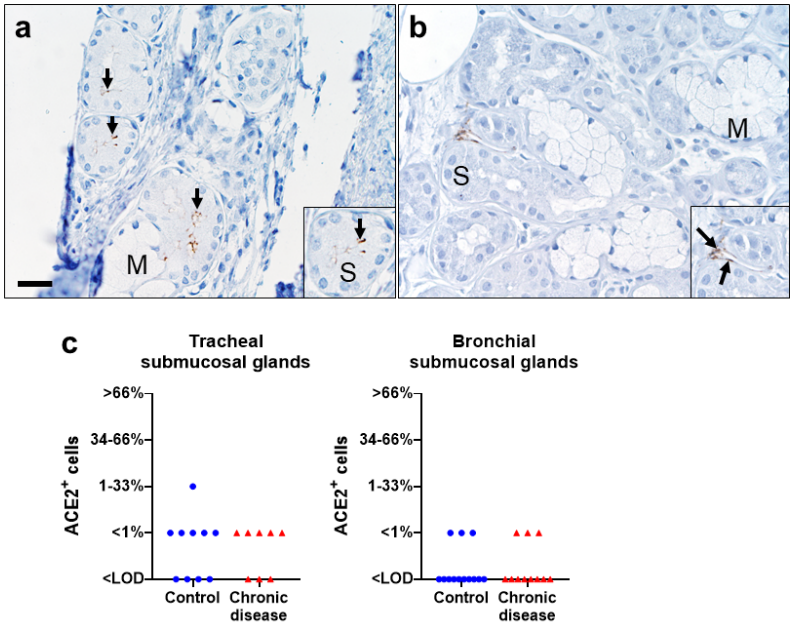

Supplemental Figure 3. Representative tissue section from submucosa of large airways (trachea/bronchi) showing ACE2 protein localization (brown color, black arrows) (**a, b**) and scores (**c**). **a**) Submucosal glands had uncommon to localized apical ACE2 protein (arrows) in serous (S) cells, but not mucous (M) cells. **b**) Submucosal glands also had absent to uncommon ACE2 protein (arrows) in the interstitium that centered on vascular walls and endothelium. This vascular staining was uncommonly seen in lung too and corresponded to the low levels seen transcripts for these endothelial cells (Supplemental Figure 1A-B). Note the absence of ACE2 staining in serous (S) or mucous (M) cells of the gland (**b**). **c**) ACE2 protein scores for each subject for serous cells in submucosal glands from trachea and bronchi, in control versus chronic disease groups (P>0.9999, 0.9999, respectively, Mann-Whitney U test). Bar = 25 μm. LOD: Limit of detection.

Supplemental Figure 4

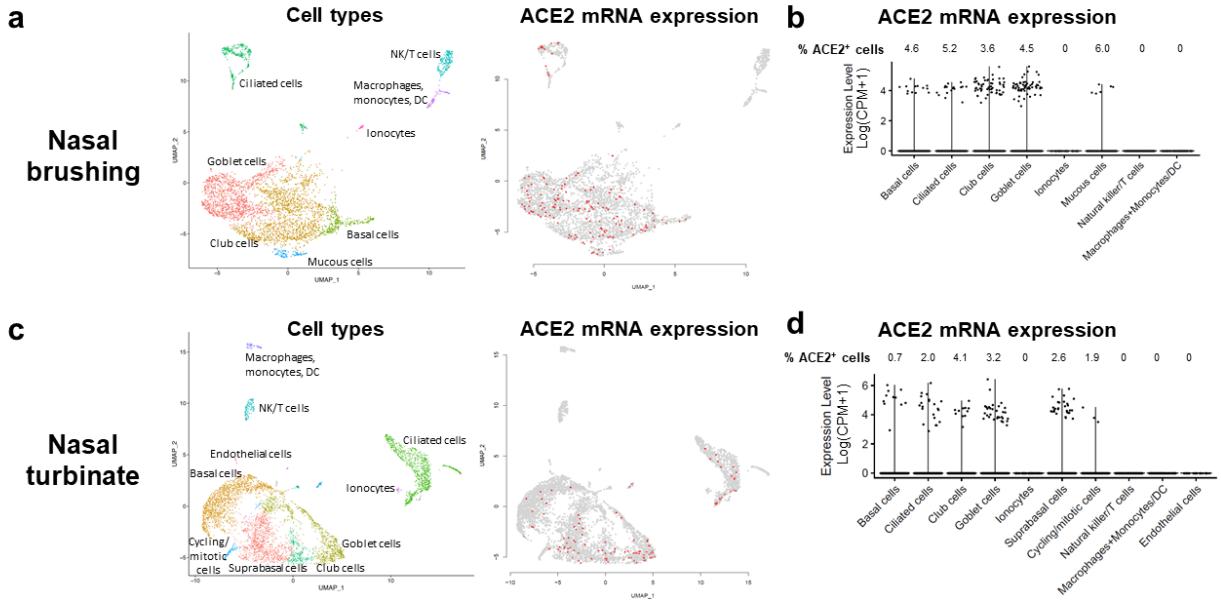

Supplemental Figure 4. Single-cell RNA sequencing reanalyses of ACE2 expression in nasal brushing (**a, b**) and nasal turbinate (**c, d**) [14]. **a, c**) Uniform manifold approximation and projection (UMAP) visualizations. Cells were clustered using a shared nearest neighbor (SNN) approach. Cell types associated with each cluster were identified by determining marker genes for each cluster. Each data point denotes a cell. On the right panels, cells expressing ACE2 are shown in red. **b, d**) Violin plots representing ACE2 expression. In nasal turbinate and nasal brushing, percentage of $ACE2^+$ cells within each cell type shows ACE2 expression on epithelial cells. Each data point denotes a cell, most cells have no expression (0). DC: dendritic cells. NK: Natural killer. CPM: Counts per million.

568 **Supplemental Table 1. ACE2 protein reported in surface epithelium (SE) of human**

569 **respiratory tract surface epithelium.**

Reported Cases (n)	Primary Ab	SN	T	B	Br	Al	Summary comments
Non-diseased lungs / nasal (5 each); diseased lungs (5) [12]	Polyclonal	SE (C++, basal cells in squamous epithelium)	n.d.	SE (C+)	n.d.	AT1 (C++); AT2 (C++)	Abundant ACE2 protein in lung epithelia
Non-diseased lungs (5) [13]	Undefined	n.d.	SE (C+, A+)	SE (C+, A+)	n.d.	"Alveoli" (A+) Mac (A+)	ACE2 is present on epithelia in several parts of the respiratory tract and macrophages
Lung (undefined) [10]	Polyclonal	n.d.	n.d.	SE (C+, N+, M+)	n.d.	AT1− AT2 (N+)	ACE2 is present in bronchial epithelium, AT2 cells and macrophages
Sinus (undefined) and Lung (undefined, same tissues as above) [11]	Polyclonal	SE (N++)	SE (−)	SE (C+, N++)	n.d.	AT1− AT2 (N++)	ACE2 is present in sinus and bronchial epithelium, AT2 cells and macrophages

570

571 Non-diseased: The cause of death was not directly related to lung disease

572 n.d.: Not described

573 Tissues: Sinonasal (SN), trachea (T), bronchi (B), bronchioles (Br), and alveoli (Al)

574 Cellular localization: cytoplasmic (C), nuclear (N), apical membrane (A)

575 Cells: Surface epithelium (SE), alveolar type I cells (AT1), alveolar type II cells (AT2), alveolar

576 macrophages (Mac)

577 ACE2 protein (based on published reports/figures): negative (−), weak (+), moderate to abundant

578 (++)

579

580 **Supplemental Table 2. Donor demographics and ACE2 distribution scores for each tissue**

581 **region.**

Case #	Group	Age (yrs)	Sex	Comorbidities	Trachea	Bronchi	Bronchioles	Alveoli
1	Control	5	F	Trauma	NA	2	2	1
2	Control	57	M	Arrhythmia	0	0	0	1
3	Control	31	M	Stroke (Joubert syndrome)	1	1	0	0
4	Control	53	F	Trauma	NA	0	0	1
5	Control	2	M	Brain hemorrhage	0	0	0	1
6	Control	2	M	Trauma	0	0	1	2
7	Control	0.5	M	Spinomuscular atrophy	NA	0	1	0
8	Control	71	M	Stroke, Parkinson's disease, nonsmoker	0	1	1	0
9	Control	4	F	Trauma	0	0	0	2
10	Control	1.2	M	Trauma	0	NA	1	1
11	Control	53	F	Trauma, nonsmoker	0	0	2	0
12	Control	26	F	NA	0	NA	0	0
13	Control	27	F	NA	NA	0	1	0
14	Control	64	M	NA	NA	1	1	0
15	Chronic disease	53	F	Smoker	0	NA	0	1
16	Chronic disease	60	M	COPD, smoker	NA	NA	0	1
17	Chronic disease	32	M	COPD, smoker	0	0	0	1
18	Chronic disease	68	M	COPD	NA	1	0	1
19	Chronic disease	68	F	COPD	NA	NA	1	1
20	Chronic disease	9	M	Asthma	0	0	0	1
21	Chronic disease	25	F	Cystic fibrosis	NA	0	0	0
22	Chronic disease	47	F	Cardiovascular disease	1	2	2	1
23	Chronic disease	27	M	Cystic fibrosis	0	NA	NA	1
24	Chronic disease	50	F	Cardiovascular disease, diabetes, asthma	NA	0	0	0
25	Chronic disease	37	M	Drug use, smoker	0	0	0	0
26	Chronic disease	38	M	Asthma (status asthmaticus)	0	0	0	0
27	Chronic disease	32	M	Cystic fibrosis	NA	NA	0	1
28	Chronic disease	58	F	Cardiovascular disease, diabetes, NASH	0	0	0	1
29	Chronic disease	19	F	Cystic fibrosis	NA	0	0	0

582

583 NA: Not available for analyses / COPD: Chronic obstructive pulmonary disease / NASH: Non-

584 alcoholic steatohepatitis.

585 Scoring: 0 = below limit of immunohistochemical detection; 1 = rare (<1%); 2 = <33%; 3 = 34-

586 66%; 4 = >66% of cells.

587

588 **Supplemental Table 3. Parameters for immunohistochemistry on fixed tissues.**

Target	Primary Antibody	Antigen Retrieval	Secondary Reagents
Allograft Inflammatory Factor 1 (AIF1)	Anti-AIF1 polyclonal (#019-19741, Wako Pure Chemical Industries, Ltd., Richmond, VA USA) in diluent 1:1000 x 1 hour	HIER, Citrate buffer pH 6.0, 110˚C for 15 min; 20 min cool down (Decloaking Chamber Plus, Biocare Medical, Concord, CA USA)	Dako EnVision+ System-HRP Labeled Polymer Anti-rabbit, 30 min (Dako North America, Inc., Carpentaria, CA USA) AEC chromogen, counterstain.
Angiotensin-Converting Enzyme 2 (ACE2)	Anti-ACE2, monoclonal (MAB933, R&D Systems, Minneapolis, MN USA) in diluent at 1:100 x 1 hour.	HIER, Citrate Buffer, pH 6.0, 110˚C for 15 minutes; 20 min cool down (Decloaking Chamber Plus, Biocare Medical, Concord, CA USA)	Dako EnVision+ System-HRP Labeled Polymer Anti-mouse, 60 min (Dako North America, Inc., Carpentaria, CA USA), DAB Chromogen, counterstain.
MUC5B	Rabbit anti-MUC5B polyclonal, (LSBio #LS-B8121, LifeSpan BioSciences, Inc., Seattle, WA) in Dako Antibody Diluent (Dako North America, Inc., Carpentaria, CA); 1:60,0000/30 min	HIER, Citrate buffer pH 6.0, 110˚C for 15min; 20 min cool down	Step 1: Biotinylated anti-Rabbit IgG (H+L) (Vector Laboratories, Inc., Burlingame, CA) in Dako Wash Buffer (Dako North America, Inc., Carpentaria, CA); 1:500, 30 min Step 2: Vectastain ABC Kit (Vector Laboratories, Inc., Burlingame, CA), 30min. DAB Chromogen, counterstain.
Surfactant Protein – C (SP-C)	Anti-SP-C, polyclonal (PA5-71680, Thermo Fisher Scientific, Waltham, MA USA) in diluent 1:100 x 1 hour	HIER, Citrate Buffer, pH 6.0, 110˚C for 15 minutes; 20 min cool down (Decloaking Chamber Plus, Biocare Medical, Concord, CA USA)	Dako EnVision+ System-HRP Labeled Polymer Anti-rabbit, 60 min (Dako North America, Inc., Carpentaria, CA USA), AEC chromogen, counterstain.

589

590 HIER – Heat-induced epitope retrieval

591 DAB – 3,3'-Diaminobenzidine (produces brown stain)

592 AEC - aminoethyl carbazole (produces red stain)

593 Counterstain – Harris hematoxylin (blue color)